

NASA Contractor Report 3474

NASA  
CR  
3474  
c.1



# On the Effect of Boundary Layer Growth on the Stability of Compressible Flows

Nabil M. El-Hady

LEARN COPY: RETURN TO  
AFWL TECHNICAL LIBRARY  
KIRTLAND AFB, N.M.

GRANT NSG-1645  
OCTOBER 1981

**NASA**



NASA Contractor Report 3474

# On the Effect of Boundary Layer Growth on the Stability of Compressible Flows

Nabil M. El-Hady  
*Old Dominion University*  
*Norfolk, Virginia*

Prepared for  
Langley Research Center  
under Grant NSG-1645

**NASA**

National Aeronautics  
and Space Administration

**Scientific and Technical  
Information Branch**

1981

## I. INTRODUCTION

The linear instability of small amplitude disturbances in boundary-layer flows has received considerable attention in an attempt to develop a better understanding of this aspect of the transition process. This instability is sufficiently described by the parallel stability theory, where the boundary-layer flow is assumed to be parallel. In spite of the qualitative success of this assumption, experiments have shown systematic differences from the parallel stability theory.

Apart from predicting a critical Reynolds number that is lower than that given by the parallel stability theory, evidence from the experiments show that the growth rate of the disturbance is a function of the coordinate normal to the wall in a subsonic or supersonic boundary layer. The parallel stability theory cannot predict that and consequently a detailed comparison with experiment cannot be made in a meaningful way to the necessary degree of precision, the parallel theory gives only a qualitative results. Also in cases where large pressure gradient or large amount of suction exists as in laminar flow control systems, the parallel theory fails to predict accurately the stability characteristics.

With the advancement of the numerical techniques and the possibility of solving the disturbance equations to considerable accuracy, a more critical comparison with experiments seems now possible. This demands a consistent theory describing the behavior of the disturbances over large regions of a real growing boundary layer. The nonparallel stability theory, which takes into account the dependence of the flow parameters on the chordwise coordinate (see Figure 1 for the coordinate system), as well as the

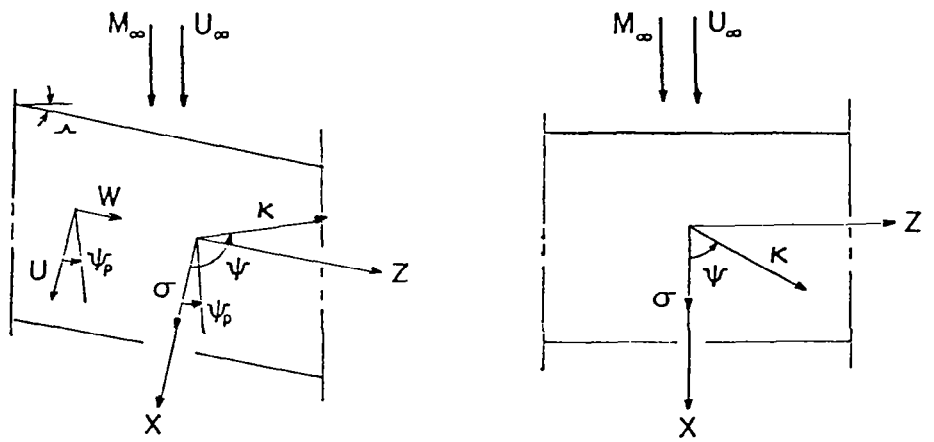


Figure 1. The Coordinate system.

velocity normal to the the wall, this theory gives a more accurate mathematical model for the development of the disturbance. The full non-parallel incompressible stability problem for two-dimensional boundary-layer flows has been solved by Bouthier<sup>1,2</sup>, Nayfeh et al<sup>3</sup>, and Gaster<sup>4</sup>, and applied to different types of boundary-layer flows<sup>5-8,22</sup>. The nonparallel compressible problem has been reported by El-Hady<sup>9</sup>, El-Hady and Nayfeh<sup>10</sup> for two-dimensional flows, and by El-Hady<sup>11,12</sup> and Nayfeh<sup>13</sup> for three-dimensional boundary layer flows. The work of Gaponov<sup>14</sup>, which appeared during writing this report, investigates only the nonparallel effects on two-dimensional disturbances.

It is the purpose of the present work to describe a formally correct method, based on the nonparallel linear theory, that examines the two- and three-dimensional stability of compressible boundary-layer flows. The method is applied to the supersonic flat plate boundary layer at Mach number 4.5, and the theoretical growth rates of disturbances are compared with the experimental results of Kendall<sup>15</sup>. The method is applied also to the infinite-span swept wing boundary-layer flow with suction at Mach number 0.82 to evaluate the effect of the nonparallel flow on the development of cross-flow instabilities.

## II. NONPARALLEL SPATIAL STABILITY THEORY

This study is concerned with the stability of small amplitude disturbances in two types of boundary-layer flows, the flat plate supersonic boundary layer, and the infinite-span swept wing transonic boundary layer with suction. In both types, the mean flow is independent of the spanwise  $z^*$ -coordinate. However, the most amplified Tollmien-Schlichting instabilities can be chordwise (two-dimensional) or oblique (three-dimensional) for the flat plate supersonic boundary layer<sup>16</sup>, but certainly oblique for the infinite-span wing transonic boundary layer. In the latter, crossflow instabilities also exist due to the presence of boundary-layer crossflow.

We consider disturbances that is generated by a steady source oscillating at the frequency  $\omega^*$  (monochromatic wave) at the curve  $x^* = 0$ . This spatial wavetrain is assumed to be of uniform amplitude in the spanwise coordinate, but with variable phase. With this in mind, we present here a formulation for the stability problem of the infinite-span wing boundary layer. All spanwise variation of the meanflow and disturbance quantities is zero.

We begin with the equations of motion for compressible flow, and introduce dimensionless quantities by using as reference, the values at the edge of the boundary layer, and a reference length  $L^*$  defined as

$$L^* = (\nu_{ex}^*/U_e^*)^{1/2} \quad (1)$$

where  $\nu^*$  is the kinematic viscosity coefficient,  $x^*$  is the distance perpendicular to the leading edge, and  $U^*$  is the velocity in the chordwise  $x^*$  - direction. Here,  $*$  denotes a dimensional quantity, and  $e$  denotes

the condition at the edge of the boundary layer. Then, the Reynolds number is defined as

$$R = U_e^* L^* / \nu_e^* = (U_e x^* / \nu_e)^{1/2} \quad (2)$$

We consider the boundary-layer flow to be weakly nonparallel, that is the meanflow quantities are weakly varying functions of the chordwise coordinate, and the normal velocity component  $V$  is small compared to the velocity components  $U$  (chordwise) and  $W$  (spanwise). The meanflow variation is scaled by introducing the new variable  $X$  defined as

$$X = \epsilon x, \quad \epsilon = 1/R \quad (3)$$

then we write the mean-flow velocity field as

$$U(X,y), \quad V(X,y), \quad W(X,y) \quad (4a)$$

and the mean-flow temperature, density, viscosity, and pressure fields as

$$\theta(X,y), \quad \bar{\rho}(X,y), \quad \bar{\mu}(\theta), \quad P(X) \quad (4b)$$

We express the mean-flow quantities in terms of mean and disturbance motions. The disturbance motions are assumed to vary slowly with the chordwise coordinate. They are described by an amplitude which is uniform in the spanwise coordinate and a phase function  $\phi(x,z,t)$  that vary with both  $x$  and  $z$  coordinates as well as time  $t$ . We use the method of multiple scales<sup>17</sup> and expand the disturbance components in power series of  $\epsilon$ . Then the mean-flow quantities in dimensionless form can be written as

$$u = U(X,y) + [u_0(X,y) + \epsilon u_1(X,y)] \exp(i\phi) \quad (5a)$$

$$v = V(X,y) + [v_0(X,y) + \epsilon v_1(X,y)] \exp(i\phi) \quad (5b)$$

$$w = W(X,y) + [w_0(X,y) + \epsilon w_1(X,y)] \exp(i\phi) \quad (5c)$$

$$p = P(X) + [P_0(X,y) + \epsilon P_1(X,y)] \exp(i\phi) \quad (5d)$$

$$\rho = \bar{\rho}(X,y) + [\rho_0(X,y) + \epsilon \rho_1(X,y)] \exp(i\phi) \quad (5e)$$

$$\theta = \bar{\theta}(X,y) + [\theta_0(X,y) + \epsilon \theta_1(X,y)] \exp(i\phi) \quad (5f)$$

$$\mu = \bar{\mu}(\theta) + \frac{d\bar{\mu}}{d\theta} [\theta_0(X,y) + \epsilon \theta_1(X,y)] \exp(i\phi) \quad (5g)$$

Where the real frequency is

$$\omega(X) = -\phi_t \quad (6)$$

and the complex wavenumber components are

$$\alpha(X) = \phi_x \quad (7)$$

$$\beta(X) = \phi_z \quad (8)$$

Here the subscripts  $t$ ,  $x$ , and  $z$  denote partial differentiation with respect to these variables. Equations (7) and (8) define a complex wavenumber vector as

$$\vec{K}(X) = \text{grad } \phi \quad (9)$$

and hence

$$\text{Curl } \vec{K} = 0 \quad (10)$$

We substitute Eqs. (3)-(8) into the dimensionless equations of motion, and transform the spatial and temporal derivatives from  $x$ ,  $z$ , and  $t$  to  $\chi$  and  $\phi$ . We eliminate nonlinear terms of the product of the disturbance quantities since they are assumed to be small, subtract the average equations of the mean-flow, and equate terms order  $\epsilon^0$  and order  $\epsilon$ .

The eigenvalue problem that is formed by the zero-order equations can be written as

$$\{Z_{0y}\} - [a] \{Z_0\} = 0 \quad (11)$$

with the boundary conditions

$$Z_{01} = Z_{03} = Z_{05} = Z_{07} = 0 \quad \text{at } y = 0 \quad (12)$$

$$Z_{01}, Z_{03}, Z_{05}, Z_{07} \rightarrow 0 \quad \text{as } y \rightarrow \infty \quad (13)$$

where

$$\begin{aligned} Z_{01} &= u_0, \quad Z_{02} = u_{0y}, \quad Z_{03} = v, \quad Z_{04} = p, \\ Z_{05} &= \theta_0, \quad Z_{06} = \theta_{0y}, \quad Z_{07} = w, \quad Z_{08} = w_{0y} \end{aligned} \quad (14)$$

and the elements of the matrix  $a$  are defined in Appendix I. The boundary condition (13) assumes that the disturbances are subsonic. It is reminded here that stability formulation is presented for the infinite-span-wing boundary layer, where Eqs. (11) consist of eight first order system of differential equations. The same set of equations governs the three-dimensional stability of the flat plate boundary layer, except that the spanwise mean velocity component  $W$  will disappear from the elements of the coefficient matrix  $a$  of Eqs. (11). However, the two-dimensional stability of the flat plate boundary layer is governed by a set of six order systems of differential equations.

Equations (11) - (13) are integrated numerically<sup>11</sup> to provide a solution in the form

$$\{Z_0\} = A(X) \{\zeta(X,y)\} \quad (15)$$

where  $\zeta$  is an eigenmode solution vector that is normalized in some specified but arbitrary manner, and  $A$  is a complex amplitude function which is yet to be determined.

Using Eq. (15), we write the non-homogeneous first-order equations as

$$\{Z_{1y}\} - [a] \{Z_1\} = \{b_1\} A + \{b_2\} A_X \quad (16)$$

$$Z_{11} = Z_{13} = Z_{15} = Z_{17} = 0 \quad \text{at } y = 0 \quad (17)$$

$$Z_{11}, Z_{13}, Z_{15}, Z_{17} \rightarrow 0 \quad \text{as } y \rightarrow \infty \quad (18)$$

where the elements of the vectors  $b_1$  and  $b_2$  are given in Appendix II. They are known functions of  $\alpha$ ,  $\beta$ ,  $\zeta$ , and the meanflow quantities. By using the adjoint function  $\zeta^*(X,y)$ , which is a solution of the adjoint homogeneous problem;

$$\{\zeta^*_{y}\} + [a] \{\zeta^*\} = 0 \quad (19)$$

$$\zeta^*_2 = \zeta^*_4 = \zeta^*_6 = \zeta^*_8 = 0 \quad \text{at } y = 0 \quad (20)$$

$$\zeta^*_2, \zeta^*_4, \zeta^*_6, \zeta^*_8 \rightarrow 0 \quad \text{as } y \rightarrow \infty \quad (21)$$

we write the solvability condition of Eqs. (16) - (18) as

$$[\{b_1\} A + \{b_2\} A_X] \{\zeta^*\}^T dy = 0 \quad (22)$$

where T indicates the transpose of the vector. We can write Eq. (22) in the following form for the evolution of A:

$$A_X = i \tilde{\alpha}(X) A \quad (23)$$

where

$$i \tilde{\alpha} = - \int_0^{\infty} \{b_1\} \{\zeta^*\}^T dy / \int_0^{\infty} \{b_2\} \{\zeta^*\}^T dy \quad (24)$$

The solution of Eq. (24) can be written as

$$A = A_0 \exp \left[ i \int \tilde{\alpha}(X) dX \right] = A_0 \exp \left[ i \epsilon \int \tilde{\alpha}(X) dx \right] \quad (25)$$

where  $A_0$  is a constant.

The evolution of the wavenumber components  $\alpha$  and  $\beta$  are determined as follows. We replace  $Z$  with  $\zeta$  in Eqs. (11) - (13), differentiate the result with respect to  $X$  and use the symmetry condition (10) to obtain

$$\{\zeta_{XY}\} - [a] \{\zeta_X\} = i \{b_2\} \alpha_X + \{d\} \quad (26)$$

with homogeneous boundary conditions similar to those given in Eqs. (12) and (13), the vector  $d$  is defined in Appendix III. Applying the solvability condition to Eqs. (26) we obtain

$$\alpha_X = - \int_0^{\infty} \{d\} \{\zeta^*\}^T dy / i \int_0^{\infty} \{b_2\} \{\zeta^*\}^T dy \quad (27)$$

Similarly, differentiating Eqs. (11) - (13) with respect to Z and using the symmetry condition (10) we obtain

$$\beta_x = 0 \quad (28)$$

The evolution of  $\alpha$  and  $\beta$  is governed by Eqs. (27) and (28). Equation (28) indicates that the complex spanwise wavenumber  $\beta$  will be constant along the chordwise coordinate.

Therefore, to the first approximation, Eqs. (5), (17), (25), and (27) gives

$$\{z_0\} = A_0 \{\phi(x,y)\} \exp [i \int (\alpha + \epsilon \tilde{\alpha}) dx + i\beta z - i\omega t] \quad (29)$$

The effect of the growing boundary layer is reflected in Eq. (29) by perturbing  $\alpha$  to  $\epsilon \tilde{\alpha}$  and by making the eigen solution function of the chordwise coordinate in addition to being function of the normal coordinate. In Eq. (29) both  $\beta$  and  $\omega$  are constants.

### III. NUMERICAL PROCEDURE

One can write the real and imaginary parts of  $\alpha$  and  $\beta$  as function of a real wave number vector  $\vec{k}$  with direction  $\Psi$ , and a real spatial growth rate vector  $\vec{\sigma}$  with direction  $\bar{\Psi}$ ; that is

$$\text{Re}(\alpha) = k \cos \Psi \quad , \quad \text{Im}(\alpha) = -\sigma \cos \bar{\Psi} \quad (30)$$

$$\text{Re}(\beta) = k \sin \Psi \quad , \quad \text{Im}(\beta) = -\sigma \sin \bar{\Psi} \quad (31)$$

For a given  $R$ , we specify  $\text{Re}(\beta)$  (or the angle  $\Psi$ ),  $\text{Im}(\beta)$ , and a dimensionless frequency defined as

$$F = 2 \pi f^* v_\infty^* / U_\infty^{*2} \quad (32)$$

where  $f^*$  is the dimensional frequency in CPS, and  $\infty$  denotes freestream conditions. In all numerical results presented in this paper, we chose  $\text{Im}(\beta) = 0$  at the leading edge, that is  $\bar{\Psi} = 0$ . We note that Eq. (28) requires that  $\text{Im}(\beta)$  will remain constant along the chordwise coordinate.

The eigenvalue problem (11) - (13) is integrated numerically from  $y = y_e$  to the wall using a variable step size algorithm based on the Runge-Kutta-Fehlberg fifth-order formulas, coupled with an orthonormalization procedure.<sup>18</sup> Following the same procedure, the adjoint problem (19)-(21) is solved for the adjoint function  $\zeta^*$ , except that it has the same eigenvalues as the homogeneous problem (11) - (13).

To determine  $\tilde{\alpha}(x)$ , we need to evaluate  $\zeta_x$  and  $\alpha_x$ . The  $\alpha_x$  is calculated using Eq. (27), while  $\zeta_x$  are evaluated by solving the homogeneous part of Eq. (26) with homogeneous boundary conditions.

Using Eq. (29), the spatial growth rate of the disturbance, defined as  $\text{Re}(Z_x/Z)$ , can be written as

$$\sigma = -\text{Im}(\alpha) - \epsilon [\text{Im}(\tilde{\alpha}) - \text{Re}(\zeta_x/\zeta)] \quad (33)$$

The first term is the spatial growth rate in a parallel flow, while the second is a correction due to nonparallel effects. The dependence of the eigen function  $\zeta$  in the chordwise coordinate in the nonparallel theory, made it possible to determine the growth rate as function of the normal coordinate as well as the disturbance flow variable.

Because a hot wire anemometer in a supersonic stream responds to both mass-flow and total temperature disturbances, we use these disturbance flow variables to demonstrate the theoretical results. The amplitude function of the mass-flow disturbance is given by

$$\rho u = [U(\gamma M_\infty^2 \zeta_4 - \zeta_5/\theta) + \zeta_1] / \theta \quad (34)$$

and the amplitude function of the total temperature disturbance is given by

$$T = \zeta_7 + (\gamma - 1) M_\infty^2 U \zeta_1 \quad (35)$$

#### IV. FLAT PLATE BOUNDARY LAYER AT $M_\infty = 4.5$

In this section, we compare the theoretical growth rates of a three-dimensional disturbances with  $\psi = 55^\circ$ , and a two-dimensional disturbance ( $\psi = 0^\circ$ ) in the flat plate supersonic boundary layer with the experimental findings of Kendall<sup>15</sup>.

##### A. Theoretical Results

For a three-dimensional disturbance with wave angle  $\psi = 55^\circ$  and frequency  $F = 30 \times 10^{-6}$  (first mode), Fig. 2 shows theoretical results of the variation of the mass-flow amplitude  $|\rho_u|$  as well as the total temperature amplitude  $|T|$  with normal coordinate  $y$  at  $R = 1550$ . Both are normalized with  $|\rho_u|_m$ , the maximum value of  $|\rho_u|$ . The variation of  $|\rho_u|$  and  $|T|$  with  $y$  is typical for the unstable frequency range at  $R = 1550$ , except that the  $y$ -location of the peak value varies slightly with frequency. The peak location of  $|\rho_u|$ , for example, changes from  $y = 12.7$  at  $F = 5 \times 10^{-6}$  to  $y = 12.0$  at  $F = 75 \times 10^{-6}$ , the peak value is not sharp in general, but extends over a considerable normal distance as shown in figure 3. While  $|T|$  has two peak values,  $|\rho_u|$  has only one peak that is twice as much as the higher peak value of  $|T|$  and occurs at different  $y$ -locations.

The normal structure of the different amplitude functions evolves differently as the disturbance travels downstream. Hence, at each normal location,  $|\rho_u|$  and  $|T|$  vary differently in the chordwise direction. Because of this behaviour, growth rates based on the amplitudes  $|\rho_u|$  and  $|T|$  are functions of  $y$  at fixed  $x$ -locations. This is shown in Fig. 2 as  $\sigma|\rho_u|$  and  $\sigma|T|$  respectively. The discontinuity in  $\sigma|\rho_u|$  curve at  $y = 6$  is due to a near zero amplitude of  $|\rho_u|$  at this  $y$ -location.

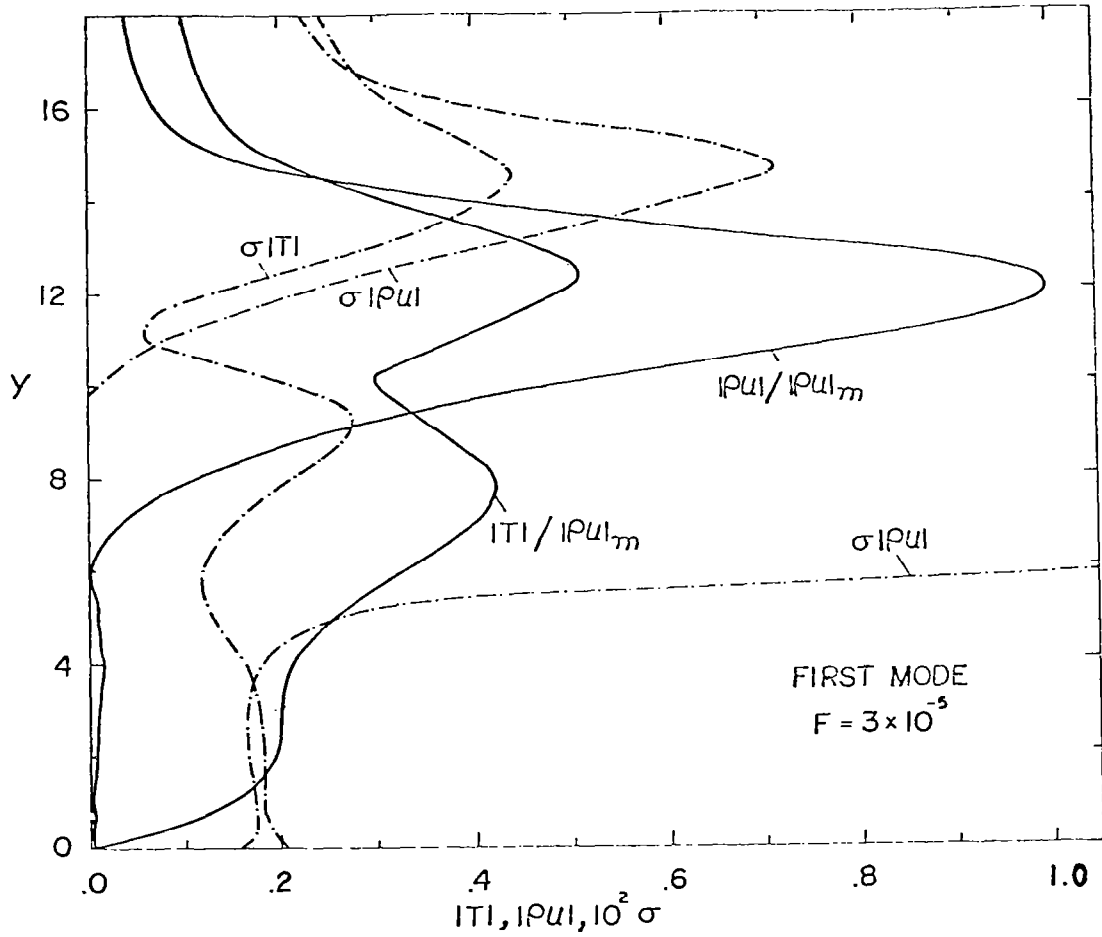


Figure 2. Variation of the amplitudes and growth rates of the mass flow and total temperature disturbances with the normal coordinate at  $R = 1550$  (first mode).

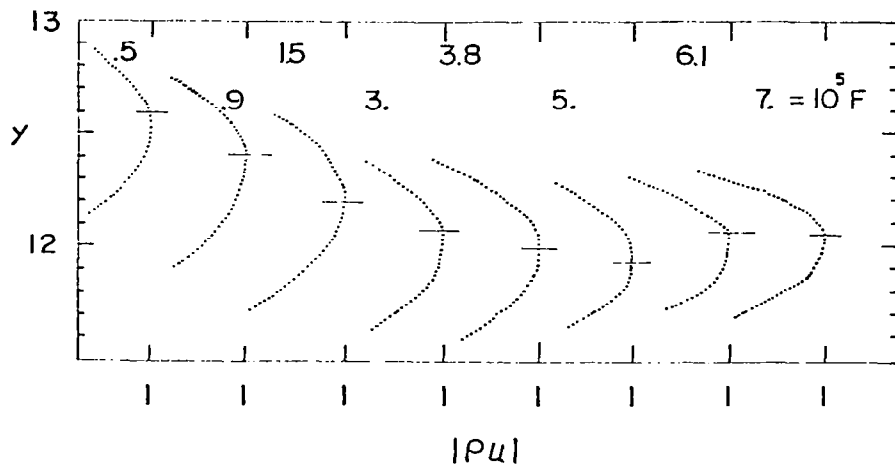


Figure 3. Normal location of the peak value of the mass-flow amplitude at  $R = 1550$  and different frequencies (first mode).

At the same chordwise location,  $R = 1550$ , we calculated the growth rates of a two-dimensional disturbance at higher frequencies (second mode). For the frequency  $F = 130 \times 10^{-6}$ , fig. 4 shows the variation of the mass-flow amplitude  $|\rho u|$  and the total temperature amplitude  $|T|$  (normalized with the maximum value of  $|\rho u|$ ), together with the variation of the growth rates  $\sigma|\rho u|$  and  $\sigma|T|$  with  $y$ -coordinate. Again, the variation of  $|\rho u|$  and  $|T|$  with  $y$  is typical for the unstable frequency range at  $R = 1550$ , with the  $y$ -location of the peak value varies slightly with frequency. The peak location of  $|\rho u|$  varies from  $y = 12.40$  at  $F = 120 \times 10^{-6}$  to  $y = 12.05$  at  $F = 158 \times 10^{-6}$ . Figure 5 shows the variation of the peak location of  $|\rho u|$  with  $y$  for this frequency range, and shows that wide peaks exist at some frequencies. In contrast with the first mode, fig. 4 shows that for the second mode the peak value of  $|T|$  (the higher one) is twice as much as the peak value of  $|\rho u|$  and occurs at different  $y$ -locations.

#### B. Comparison With Experiment

It is worth noting that, like the theory, the experiment also gives different stability conditions depending on the normal location of the measurements as well as the disturbance variable measured.

Here we compare the theoretical results with the experimental findings of Kendall<sup>15</sup>. This experiment possesses some advantages that made it the most suitable for comparison with the linear stability theory. The experiment was performed in the JPL 20-inch wind tunnel where the tunnel wall boundary layer were laminar. A small disturbance of almost pure frequency was produced by a glow-discharge generator, and introduced at an angle  $\psi = 0^\circ$  and  $\Psi = 55^\circ$ . The chordwise growth rate of the disturbances were determined for boundary-layer flow at Mach number 4.5 by following the maximum amplitude point. Three-dimensional disturbances, introduced at  $\Psi = 55^\circ$ , were found to grow nearly equal at various spanwise  $z$ -locations.

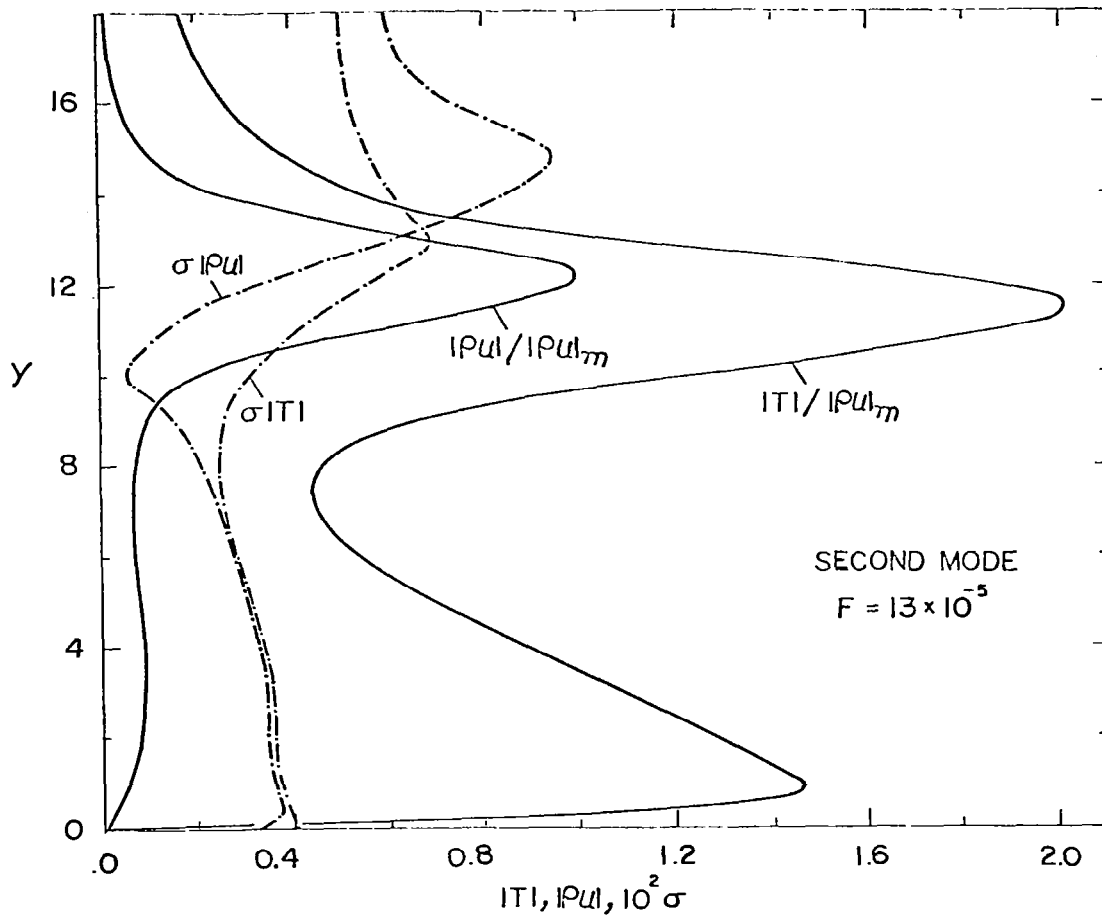


Figure 4. Variation of the amplitudes and growth rates of the mass flow and total temperature disturbances with the normal coordinate at  $R = 1550$  (second mode).

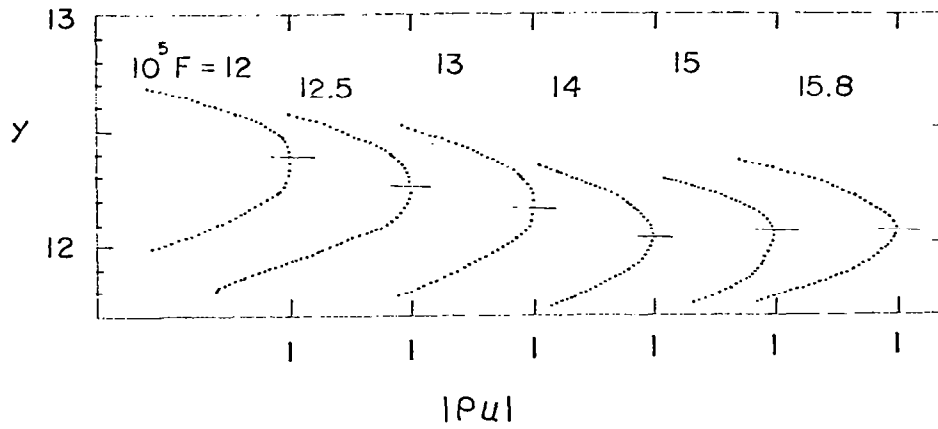


Figure 5. Normal location of the peak value of the mass-flow amplitude at  $R = 1550$  and different frequencies (second mode).

A hot wire in a supersonic flow responds to both mass-flow and total temperature disturbances with a ratio depending on the sensitivity coefficients that are determined by mean-flow conditions and the mean temperature of the hot wire. Unless measurements are conducted following a contour of constant  $y$ -location ( $y^*/L^*$  constant), sensitivity of the hot wire to changes in the mean-flow conditions cannot be avoided. Also, the hot wire response when operated at high constant overheat is proportional to the mass-flow disturbance, its sensitivity to the total temperature disturbance is minimized.

In Kendall experiment, the distribution of the measured disturbance amplitudes across the boundary layer were almost similar at different  $x$ -locations. Hence, the maximum amplitude points followed in the experiment had a contour of almost constant  $y$ -location, and sensitivity of the hot wire to changes in the mean-flow conditions was minimum. The hot wire was operated at high constant overheat to minimize its sensitivity to total temperature disturbance. Hence, energy fluctuations obtained by traversing the hot wire through the boundary layer at different  $x$ -locations for particular frequency, have been interpreted as being nearly proportional to the mass-flow disturbance amplitude.

Figure 6 shows theoretical growth rates of a three-dimensional disturbance with wave angle  $\Psi = 55^\circ$  (first mode) as function of the dimensionless frequency  $F$  at  $R = 1550$ . Parallel results, that is neither function of the normal coordinate nor the disturbance flow variable, is indicated by a dashed line, it coincides with the results of Mack given in reference 19. Nonparallel growth rates, indicated by a solid line, are calculated applying Eq (33) at the  $y$ -location where the mass-flow disturbance has a maximum. Kendall measurements of the growth rates following the maximum of a disturbance amplitude detected by the hot wire

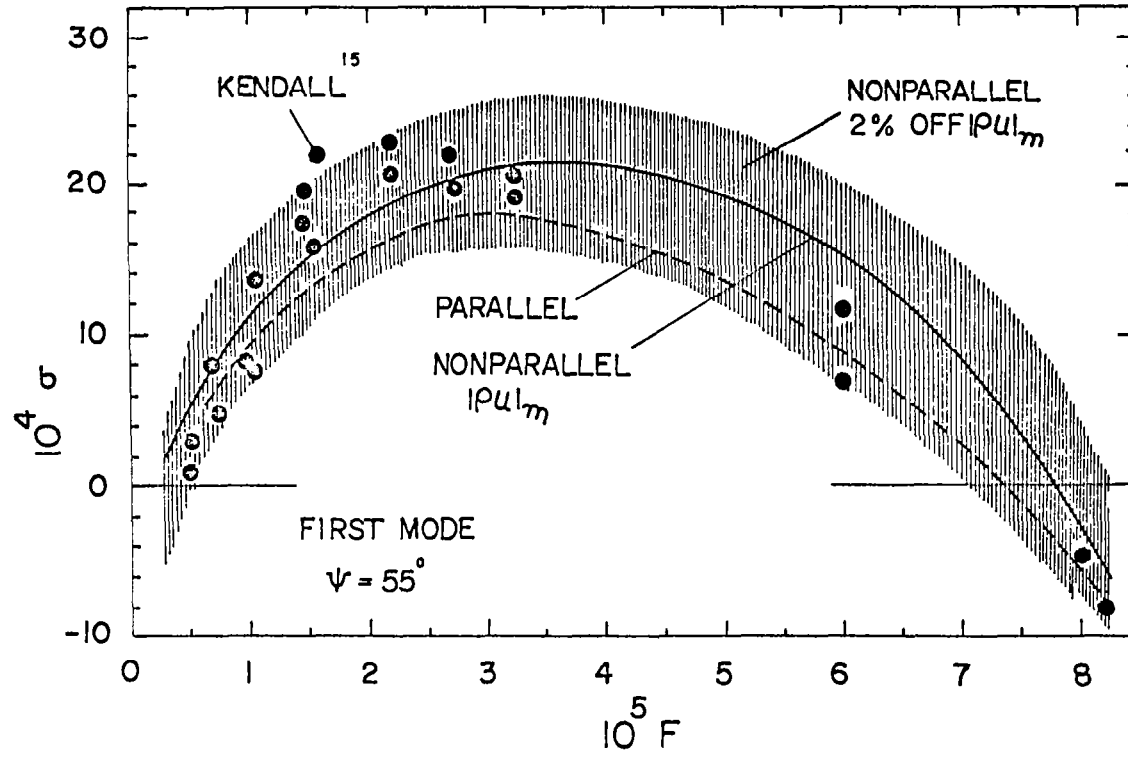


Figure 6. Variation of the growth rates of a three-dimensional disturbances,  $\psi = 55^\circ$  (first mode) with frequency, at  $R = 1550$ .

are given also in the same figure for comparison. Nonparallel results enhances the comparison between the theory and experiment by shifting the theoretically predicted growth rates to higher values compared to parallel results. However, higher growth rates are given by the experiment in the frequency range from  $10 - 35 \times 10^{-6}$ .

Figure 7 shows the theoretical growth rates of a second mode disturbance with  $\Psi = 0^\circ$ , as function of frequency at  $R = 1550$ . Parallel results indicated by the dashed line compares with that of Mack given in reference 19. Nonparallel results, indicated by the solid line, are calculated applying Eq. (33) at the  $y$ -location where the mass-flow disturbance has a maximum. Experimental growth rates by Kendall are given also in the same figure for comparison. The maximum of the disturbance amplitude detected by the hot wire is followed in these measurements. Nonparallel results again enhances the comparison between the theory and experiment by shifting the theoretically predicted unstable frequency range to higher values compared to parallel unstable frequency range.

It should be pointed out that the location of the peak detected by the hot wire at fixed  $x$ -location was assumed to be the same for all frequencies as indicated later by Kendall<sup>20</sup>, and that slightly different experimental data could have been attained for other frequencies by searching out the peak corresponding to a particular frequency as we did in the theory. The spread of the experimental data shown in Fig. 6 and Fig. 7, and the difficulty in comparing it with the theoretical results is expected. This experiment, like others, is not designed specifically to verify the non-parallel stability theory. Hence, the effect of the nonparallel flow, probably, has contributed to the difficulty in comparison. The dependence of the hot wire response not only on the mass-flow disturbance but also on the temperature disturbance, even with a minimum unknown percentage, has

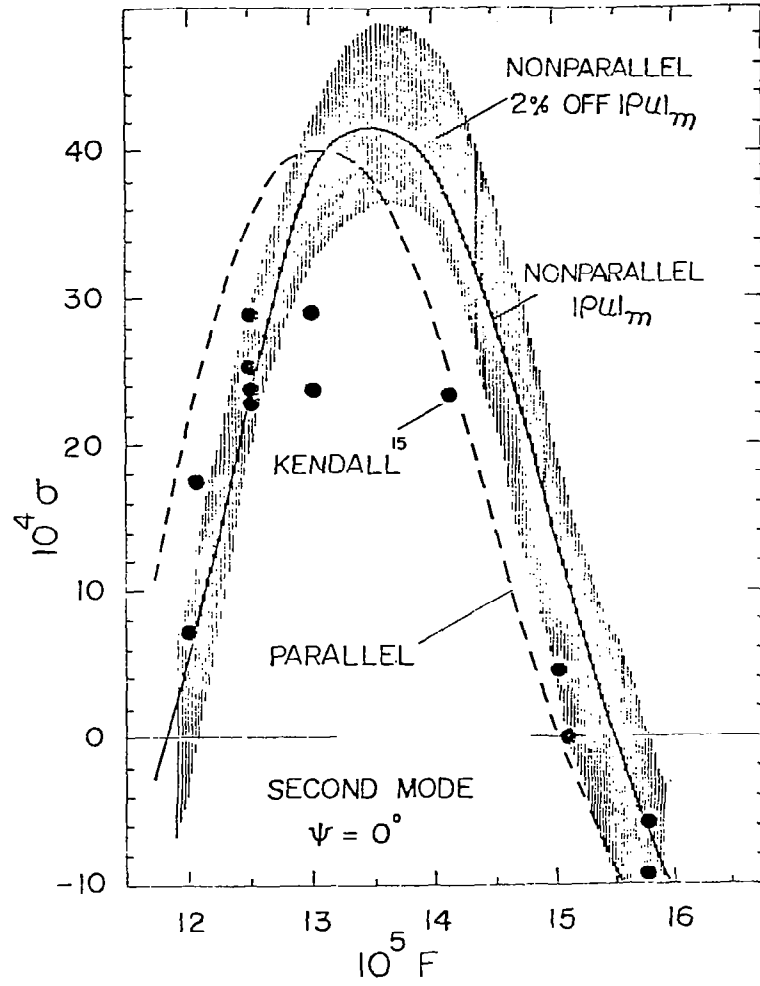


Figure 7. Variation of the growth rates of a two-dimensional disturbance,  $\psi = 0^\circ$  (second mode) with frequency, at  $R = 1550$ .

contributed also to this difficulty, figure 2 and figure 4 show that the variation of the growth rates  $\sigma|\rho u|$  and  $\sigma|T|$  are different with the y-location.

The wide peaks of  $|\rho u|$  at some frequencies make it difficult experimentally to measure the actual growth rates, specially if growth rates change rapidly around the peak location as indicated in Fig. 2 and Fig. 4. This is demonstrated in Fig. 8 which shows the variation of the growth rate of the mass flow disturbance with the normal coordinate around its peak amplitude at the frequencies  $F = 15 \times 10^{-6}$  (first mode), and  $F = 125 \times 10^{-6}$  (second mode). Experimental growth rate measurements around these frequencies are shown in Fig. 8 to fall within the wide peak of the amplitude  $|\rho u|$  that is off 1.5-3 percent from the peak value. Changes in the growth rates of  $|\rho u|$  corresponding to an average of 2 percent deviation from the peak value is calculated for all unstable frequencies of the first and second modes. Calculated growth rates form a band that is shown by the hashed area in Figs. 6 and 7. Most of the experimental data fall within this band.

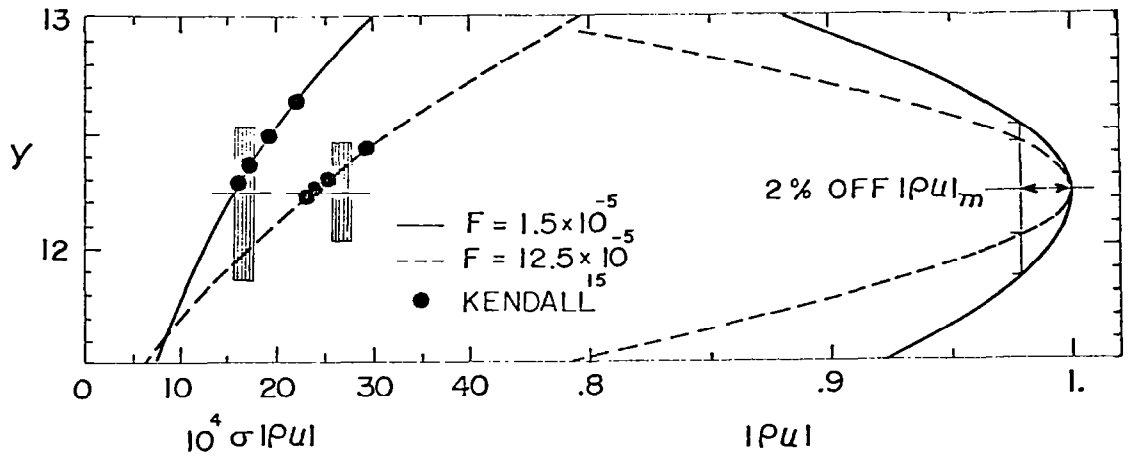


Figure 8. Variation of the growth rate of the mass flow disturbance with the normal coordinate around its peak amplitude for a first and a second mode frequencies, and the corresponding experimental growth rate measurements.

## V. BOUNDARY LAYER ON A TRANSONIC SWEEP WING

The nonparallel stability theory presented in section 2 is applied to the boundary layer with suction on a  $23^\circ$  swept infinite span wing. The airfoil section is supercritical with a normal chord  $c = 1.98$  m, and the freestream Mach number is 0.82. Parallel stability characteristics of the boundary layer on this wing have been investigated by El-Hady<sup>12</sup> and Mack<sup>21</sup>. However, some incomplete nonparallel calculations have been reported by El-Hady<sup>12</sup> for the same wing. Figure 9 shows the distribution of the pressure coefficient  $C_p$  on the upper surface of the airfoil section together with the distribution of the suction coefficient along the chord. The suction coefficient is defined as  $C_s = -\rho_0 V_c / \rho_\infty U_\infty$ , where the subscript  $_0$  denotes wall condition.

On a sweptback wing the boundary layer is three-dimensional due to the presence of boundary layer crossflow. Because the crossflow profiles are highly dynamically unstable, crossflow instabilities generate and dominate both the leading edge and rear parts of the wing where the mean crossflow components have large values.

We advance a band of initial wavelengths of constant frequency disturbances at the leading edge. These disturbances develop downstream according to Eqs. (25), (27), and (28). The spanwise component of the wavelength  $\lambda z/c$  (normalized with the normal chord) remains constant, and  $\bar{\Psi}$  remains zero if its initial value at the leading edge is zero. We calculate the parallel and nonparallel growth rates as well as the logarithmic amplitude ratios of these wave components as they develop downstream.

The logarithmic amplitude ratio  $N$  is calculated from

$$N = \ln \frac{a}{a_0} = 2 \int_{R_0}^R \sigma \, dR \quad (36)$$

where  $R_0$  is the initial Reynolds number at the lower branch of the neutral stability curve, and  $a_0$  is the corresponding disturbance amplitude. The  $\sigma$  in

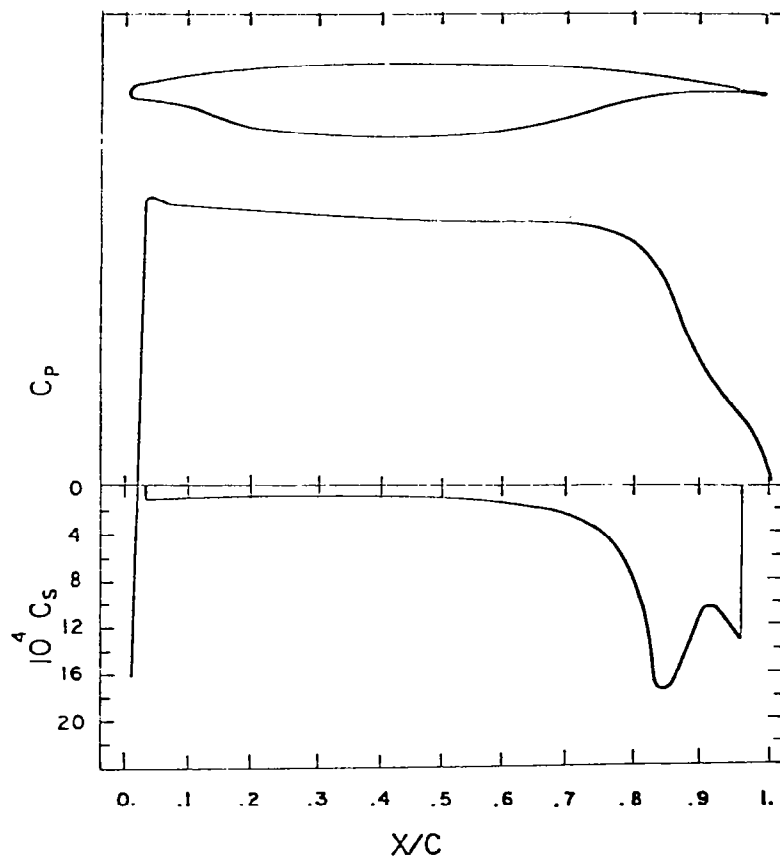


Figure 9. The distribution of the pressure and suction coefficients on the upper surface of the supercritical airfoil.

the above formula is calculated by using Eq. (33) for a constant frequency  $F$ . All results presented here are for the stationary crossflow disturbances, that is  $F = 0$ .

Calculations at the leading edge region show that a wave component with constant  $\lambda_z/c = 0.00054$  has the largest amplitude ratio, however, a wave component with constant  $\lambda_z/c = 0.0036$  has the largest amplitude ratio at the rear part of the wing. For these wave components, figure 10 shows the variation of  $|\rho u|$  and  $\sigma|\rho u|$  with  $y$  at the chordwise locations  $x/c = 0.015$  (for  $\lambda_z/c = 0.00054$ ) and  $x/c = 0.90$  (for  $\lambda_z/c = 0.0036$ ). The growth rate  $\sigma|\rho u|$  changes rapidly around the peak of  $|\rho u|$ . We use the value of  $\sigma|\rho u|$  at the  $y$ -location where  $|\rho u|$  is maximum to represent the nonparallel results as we did in the previous section.

Figures 11 and 12 show the parallel and nonparallel unstable regions of three wave components around the most unstable one (that gives the largest amplitude ratio) as well as their growth rates as they develop downstream. At the leading edge region, figure 11 indicates that the nonparallel maximum growth rates are 30 - 45 percent higher than the parallel. It is worth noting that this region extends to about 10 percent of the chord. The boundary layer is accelerated rapidly from the leading edge to  $x/c \approx 0.025$ , and small suction rates are applied to the boundary layer starting at this location. It is clear from figure 11 that in this region, parallel and nonparallel maximum growth rates are affected only by the rapidly accelerated boundary layer rather than suction rates.

At the rear part of the wing, figure 12 shows that the nonparallel maximum growth rates are 15 - 30 percent less than the parallel. The boundary layer in this region is severely decelerated and high suction rates are applied to it (peak of  $C_s \approx 0.0018$ ). The sudden drop in the parallel growth rates around  $x/c = .84$  is due to the peak suction rate. Here, maximum growth rates are affected by both the adverse pressure gradient and the severe suction rates.

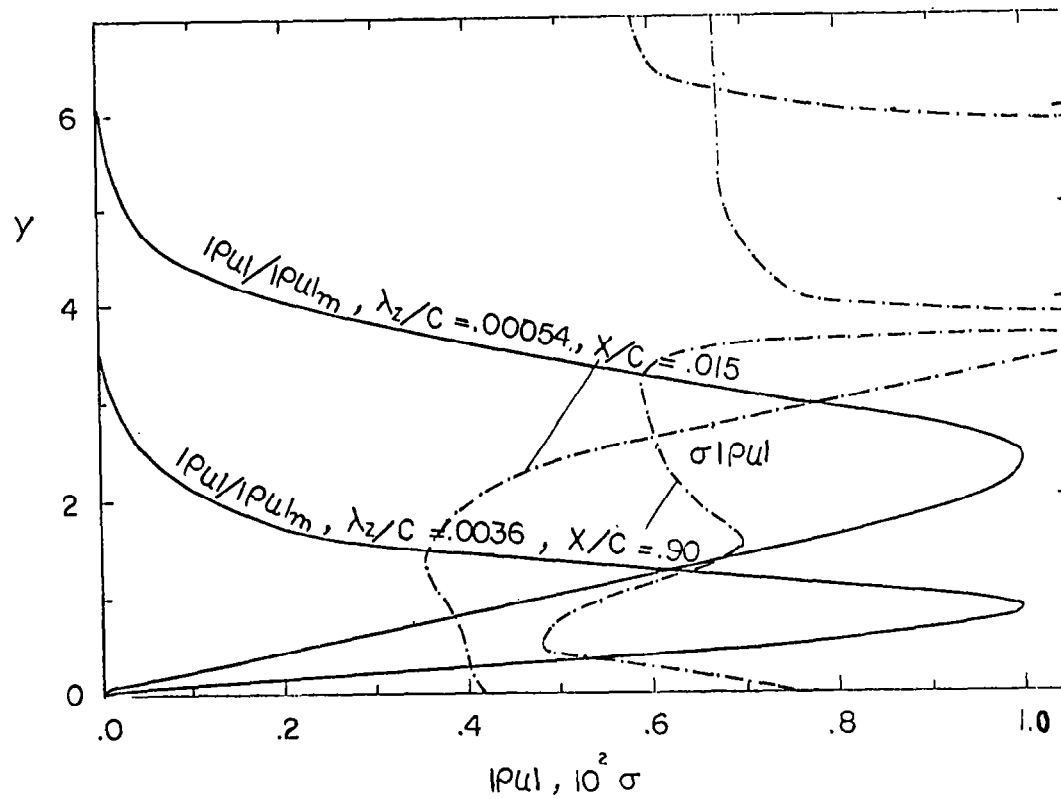


Figure 10. Variation of the amplitude and growth rates of the mass flow disturbance with the normal coordinate for the most unstable wave components at the leading edge and aft regions of the wing.

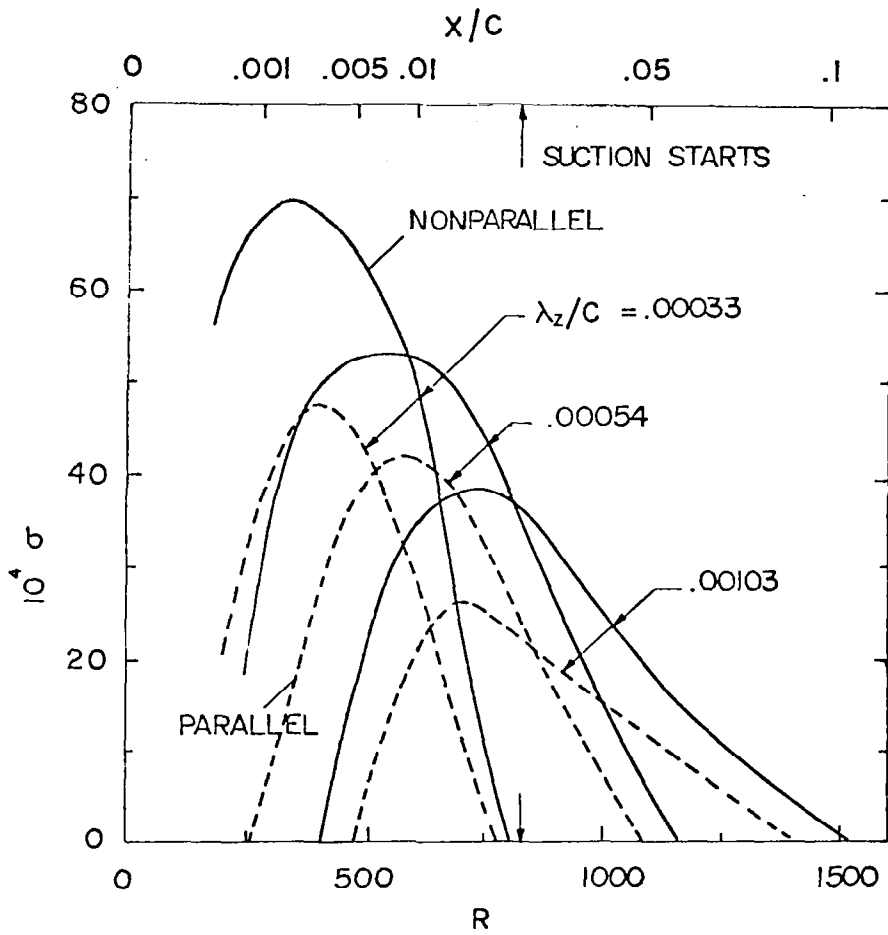


Figure 11. Growth rates of most unstable wave components of constant  $\lambda_z/c$  at the leading edge region, as they develop downstream.

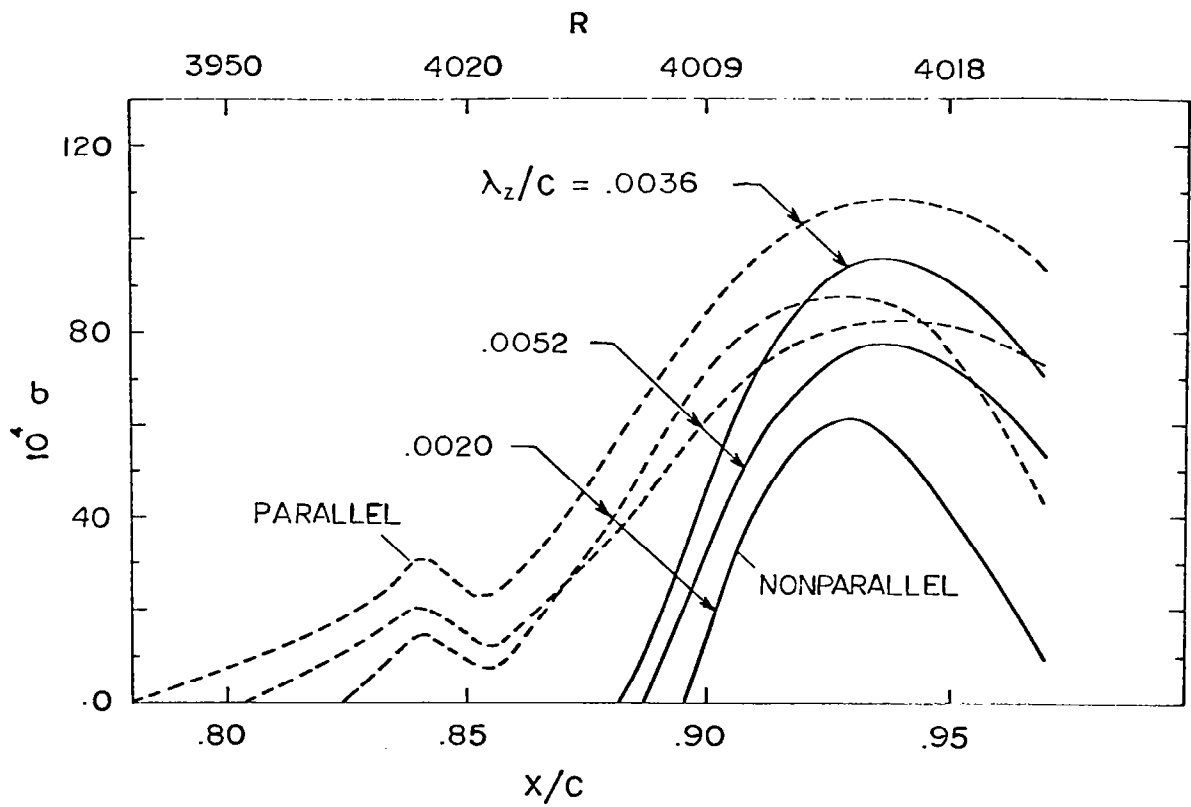


Figure 12. Growth rates of most unstable wave components of constant  $\lambda_z/c$  at the aft region, as they develop downstream.

Figure 13 shows the variation of the maximum logarithmic amplitude ratio with the wave components of constant  $\lambda_z/c$ . At the leading edge,

the boundary layer flow is destabilized due to the nonparallel flow effects. Higher nonparallel  $N_{max}$  is shown with nearly 64 percent maximum difference compared to the parallel  $N_{max}$ . On the contrary, at the rear part the boundary layer is stabilized due to nonparallel flow effects with a maximum reduction in  $N_{max}$  of nearly 43 percent. Figure 11 shows also a slight shift in the value of the most unstable wave component  $\lambda_z/c$  due to nonparallel flow effects. The most unstable wave component at the leading edge reaches its maximum amplitude at  $x/c \approx 0.032$  ( $R = 900$ ) while at the rear part, the maximum amplitude is reached at the trailing edge.

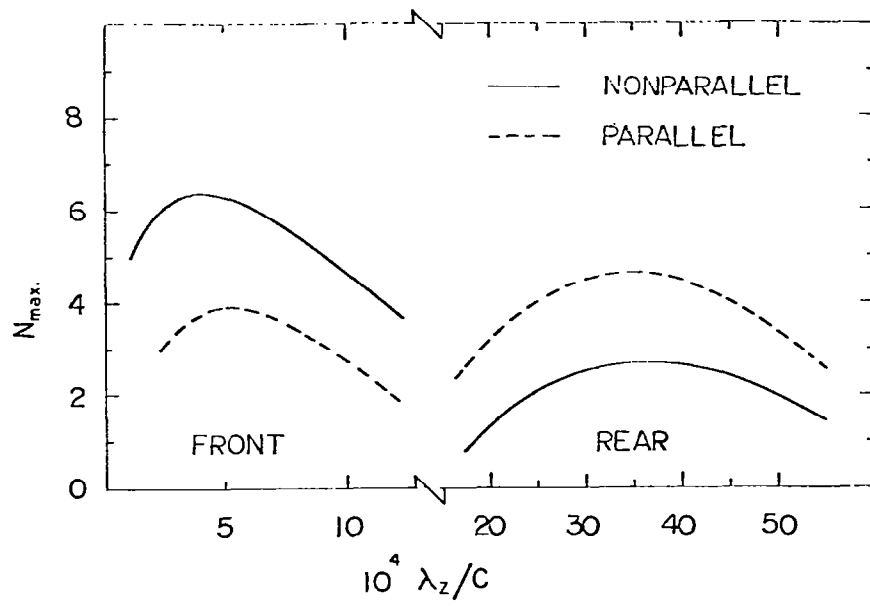


Figure 13. Variation of the maximum logarithmic amplitude ratio with wave component of constant  $\lambda_z/c$ .

## VI. CONCLUDING REMARKS

1. A method is presented to investigate the two- and three-dimensional stability of compressible boundary layer flows. The method is suitable for the flat plate boundary layer as well as the boundary layer on an infinite swept-back wing, where the meanflow is independent of the spanwise coordinate.

2. Nonparallel stability results for the flat plate boundary layer at Mach number 4.5 are in better agreement with Kendall experiments than the parallel stability results.

3. Nonparallel flow effects on crossflow instabilities are calculated for a specific infinite span transonic swept wing. The destabilizing effect at the leading edge and the stabilizing effect at the rear part is believed to be directly affected by the pressure gradients and the suction rates at this region.

## REFERENCES

1. M. Bouthier, "Stabilite lineaire des ecoulements presque paralleles, I," J. de Mecanique 11, 1 (1972).
2. M. Bouthier, "Stabilite lineaire des ecoulements prequeparalleles, II - La couche limite de Blasius," J. de Mecanique 12, 75 (1973).
3. A. H. Nayfeh, W. S. Saric, D. T. Mook, "Stability of Nonparallel Flows," Arch. Mech. Stosow 26, 401 (1974).
4. M. Gaster, "On the effects of boundary-layer growth on flow stability," J. Fluid Mech. 66, 465 (1974).
5. W. S. Saric, A. H. Nayfeh, "Nonparallel stability of boundary-layer flows," Phys. Fluids 18, 945 (1975).
6. W. S. Saric, A. H. Nayfeh, "Nonparallel stability of boundary alyers with pressure gradients and suction," in AGARD Conference Proceedings No. 224, Paper No. 6, Laminar-Turbulence Transition, Denmark 2-4 May (1977).
7. N. M. El-Hady, A. H. Nayfeh, "Nonparallel stability of two-dimensional heated boundary layer flows," in Twelfth Symposium on Naval Hydrodynamics, National Academy of Science, Washington, D.C., June 5-9 (1978).
8. A. H. Nayfeh, N. M. El-Hady, "Nonparallel stability of nonuniformly heated boundary layer flows," Phys. Fluids 23, 10 (1980).
9. N. M. El-Hady, "Effect of compressibility, suction, and heat transfer on the nonparallel stability of boundary layer flows," Ph.D. Dissertation, Virginia Polytechnic Institute & State University (1978).
10. N. M. El-Hady, A. H. Nayfeh, "Nonparallel stability of compressible boundary layer flows," Report No. VPI-E-79-13, Virginia Polytechnic Institute & State University, (1979).
11. N. M. El-Hady, "Nonparallel stability of three-dimensional, compressible boundary layers, Part I-Stability Analysis," NASA CR-3245 (1980).
12. N. M. El-Hady, "On the stability of three-dimensional, compressible, nonparallel boundary layer flows," AIAA Paper No. 80-1374, (1980).
13. A. H. Neyfeh, "Stability of three-dimensional boundary layer flows," AIAA J., 18, No. 4, 406 (1980).

14. S. A. Gaponov, "Influence of boundary layer growth on the development on disturbances in supersonic flows," *Izvestiya Akad. Nauk SSR, Mekh. Zhidkosti i Gaza*, No. 2, 26 (1980).
15. J. M. Kendall, "Supersonic boundary-layer stability experiments", in *Proceedings of Boundary Layer Transition Study Group Meeting, V. II*, ed. W. D. McCanley, Airforce Rep. BSD-TE-67-213, Aerospace Rep. TR0158 (S3816-63)-1 (1967).
16. L. M. Mack, "Boundary layer stability theory," Rep. 900-277, Rev. A, Jet Propulsion Lab., Pasadena, California (1969).
17. A. H. Nayfeh, *Perturbation Methods* (Wiley-Interscience, New York, 1973), Sec. 4.2.
18. M. R. Scott and H. A. Watts, "Computational solution of linear two-point boundary value problems via orthonormalization," *SIAM J. Num. Anal.*, 14, 40 (1977).
19. H. Schlichting, *Boundary Layer Theory* (McGraw-Hill, New York, 7th ed.) (1979).
20. J. M. Kendall, "Wind tunnel experiments relating to supersonic and hypersonic boundary layer transition," *AIAA J.*, 13, 3, 29D (1975).
21. L. M. Mack, "Compressible boundary-layer stability calculations for sweptback wings with suction," *AIAA Paper No. 81-0196*, (1981).
22. P. M. Eagles and M. A. Weissman, "On the stability of slowly varying flow: the divergent channel," *J. Fluid Mech.*, 69, 2, 241 (1975).

APPENDIX I.

The nonzero elements of the matrix  $a$  in equation (13) are:

$$a_{12} = 1$$

$$a_{21} = \frac{iR\phi}{\mu\theta} + \alpha^2 + \beta^2$$

$$a_{22} = -\frac{\mu'}{\mu}$$

$$a_{23} = \frac{RU'}{\mu\theta} - i\alpha \frac{\mu'}{\mu} (m+1) \frac{\theta'}{\theta}$$

$$a_{24} = \frac{i\alpha R}{\mu} - (m+1) \gamma M_{\infty}^2 \alpha \phi$$

$$a_{25} = (m+1) \frac{\alpha\phi}{\theta} - \frac{(\rho i')'}{\mu}$$

$$a_{26} = \frac{\rho U'}{\mu}$$

$$a_{31} = -i\alpha$$

$$a_{33} = \frac{\theta'}{\theta}$$

$$a_{34} = -i\gamma M_{\infty}^2 \phi$$

$$a_{35} = \frac{i\phi}{\theta}$$

$$a_{37} = -i\beta$$

$$a_{41} = -i\chi\alpha \left( \frac{2\mu'}{\mu} + \frac{r\theta'}{\theta} \right)$$

$$a_{42} = -i\chi\alpha$$

$$a_{43} = \chi \left( \frac{r\mu'\theta'}{\mu\theta} + \frac{r\theta''}{\theta} - \frac{iR\phi}{\mu\phi} - \alpha^2 - \beta^2 \right)$$

$$a_{44} = -i\chi r \gamma M_{\infty}^2 \left( \frac{\mu'}{\mu} + \frac{\theta'}{\theta} \right) \phi + \alpha U' + \beta W'$$

$$a_{45} = -i\chi \left( \frac{\rho}{\mu} + \frac{r}{\theta} \right) (\alpha U' + \beta W') + \frac{r\mu'\phi}{\mu\theta}$$

$$a_{46} = \frac{i\chi r\phi}{\theta}$$

$$a_{47} = -i\chi\beta \left( \frac{2\mu'}{\mu} + \frac{r\theta'}{\theta} \right)$$

$$a_{48} = -i\chi\beta$$

$$a_{56} = 1$$

$$a_{62} = -2\Gamma (\gamma - 1) M_{\infty}^2 U'$$

$$a_{63} = \frac{R\Gamma\theta'}{\mu\theta} - 2i\Gamma (\gamma - 1) M_{\infty}^2 (\alpha U' + \beta W')$$

$$a_{64} = \frac{iR\Gamma}{\mu} (\gamma - 1) M_{\infty}^2 \phi$$

$$a_{65} = \frac{iR\Gamma\phi}{\mu\phi} + \alpha^2 + \beta^2 - (\gamma - 1) M_{\infty}^2 \frac{\Gamma\mu}{\mu} (U'^2 + W'^2) - \frac{\mu''}{\mu}$$

$$a_{66} = \frac{-2\mu'}{\mu}$$

$$a_{68} = -2\Gamma (\gamma - 1) M_{\infty}^2 W'$$

$$a_{78} = 1$$

$$a_{83} = -i\beta \left( \frac{\mu'}{\mu} + (m+1) \frac{\theta'}{\theta} \right) + \frac{RW'}{\mu\theta}$$

$$a_{84} = \frac{iR\beta}{\mu} - (m+1) \beta\gamma M_{\infty}^2 \phi$$

$$a_{85} = (m+1) \frac{\beta\phi}{\theta} - \left( \frac{\mu W'}{\mu} \right)'$$

$$a_{86} = \frac{-\mu W'}{\mu}$$

$$a_{87} = \frac{iR\phi}{\mu\theta} + \alpha^2 + \beta^2$$

$$a_{88} = \frac{-\mu'}{\mu}$$

where

$$\phi = \alpha U + \beta W - \omega$$

$$\chi = 1 / \left( \frac{R}{\mu} + i\gamma M_{\infty}^2 \phi \right)$$

$$\hat{\mu} = \frac{d\mu}{d\theta}$$

$r$  is Prandtl number,  $m = 2(e - 1)/3$ , and  $r = 2(e + 2)/3$ , where  $e = 0$  corresponds to the Stokes hypothesis, it is taken  $e = 0.8$  in this analysis. The prime denotes differentiation with respect to  $y$ , and  $\mu$  is used here for the meanflow viscosity.

APPENDIX II.

The nonzero elements of the vectors  $b_1$  and  $b_2$  in equation (18) are:

$$b_{12} = C_1 I_1 + C_2 I_2$$

$$b_{13} = C_3 I_1$$

$$b_{14} = C_4 I_1 + C_5 I_1' + C_6 I_3$$

$$b_{15} = C_7 I_5$$

$$b_{18} = C_8 I_1 + C_2 I_4$$

and

$$b_{22} = C_1 I_6 + C_2 I_7$$

$$b_{23} = C_3 I_6$$

$$b_{24} = C_4 I_6 + C_5 I_6' + C_6 I_8$$

$$b_{26} = C_7 I_{10}$$

$$b_{28} = C_8 I_6 + C_2 I_9$$

where

$$C_1 = -i (m + 1) \alpha \theta, \quad C_2 = \frac{-R}{\mu}, \quad C_3 = \theta, \quad C_4 = r_X \left( \frac{\mu' \theta}{\mu} + 2\theta' \right), \quad C_5 = r_X \theta,$$

$$C_6 = \frac{R_X}{\mu}, \quad C_7 = \frac{-R\Gamma}{\mu}, \quad C_8 = -i (m + 1) \beta \theta$$

and

$$I_1 = \frac{1}{\theta^2} \left[ U_X + V' - \frac{2}{\theta} (U\theta_X + V\theta') \right] \quad \zeta_5 + U\zeta_{5X} + V\zeta_6 + \frac{1}{\theta^2} \theta_X \zeta_1$$

$$- \frac{\gamma M_\infty^2}{\theta} \left[ U_X + V' - \frac{1}{\theta} (U\theta_X + V\theta') \right] \quad \zeta_4 - \frac{\gamma M_\infty^2}{\theta} (U\zeta_{4X} + V\zeta_4') - \frac{1}{\theta} \zeta_{1X}$$

$$I_2 = \frac{ir}{R} (\alpha\mu)_X - \frac{1}{\theta} U_X \quad \zeta_1 + \frac{(2ir \mu\alpha - U)}{R} \zeta_{1X} + \frac{1}{R} (m+1) \mu X$$

$$(\zeta'_{3X} + i\beta\zeta_{7X}) + m\mu_X \zeta'_3 + \mu' \zeta_{3X} - \frac{\gamma M_\infty^2}{\theta} (UU_X + VU') \zeta_4 - \frac{V}{\theta} \zeta_2 - \zeta_{4X}$$

$$+ \frac{i\alpha\hat{\mu}}{R} (rU_X + mV') + \frac{1}{\theta^2} (UU_X + VU') - \frac{i\beta\mu}{R} W_X \quad \zeta_5 + \frac{im}{R} \beta\mu_X \zeta_7$$

$$I_3 = \frac{i}{R} (\alpha\mu)_X - \frac{V'}{\theta} \zeta'_3 + \frac{(2i \mu\alpha - U)}{R} \zeta_{3X} + \frac{1}{R} (m+1) \mu \zeta_{2X}$$

$$+ \mu_X \zeta_2 + (m+1) \hat{\mu} U'_X + U' \hat{\mu}_X + r\mu V'' \quad \zeta_5 + \hat{\mu} U' \zeta_5 + (rV' + mU_X) X$$

$$(\hat{\mu}' \zeta_5 + \mu \zeta_6) + m\mu' \zeta_{1X} - \frac{V}{\theta} \zeta'_3$$

$$I_4 = \left( \frac{i}{R} \beta\mu_X - \frac{1}{\theta} W_X \right) \zeta_1 + \frac{1}{R} i (m+1) \mu\beta \zeta_{1X} + i (\alpha\mu)_X \zeta_7$$

$$- (UW_X + VW') \left( \frac{\gamma M_\infty^2}{\theta} - \frac{\zeta_5}{\theta^2} - \frac{i\alpha\hat{\mu}}{R} W_X + \frac{i\beta\hat{\mu}}{R} (mU_X + mV') \right) \zeta_5$$

$$+ \frac{(2i \mu\alpha - U)}{R} \zeta_{7X} - \frac{V}{\theta} \zeta_8$$

$$I_5 = (\gamma - 1) M_\infty^2 \quad P_X \zeta_1 + \frac{2i\mu}{R} (\alpha\zeta_1 + \beta\zeta_7) (rU_X + mV' + W_X) - \frac{1}{\theta} X$$

$$\theta_X \zeta_1 + \frac{2(\gamma - 1)}{R} M_\infty^2 \quad U' \zeta_{3X} + (mU_X + rV') \zeta'_3 - (U\theta_X$$

$$+ V\theta') \left( \frac{\gamma M_\infty^2}{\theta} \zeta_4 - \frac{\zeta_5}{\theta^2} \right) + (\gamma - 1) M_\infty^2 (U\zeta_{4X} + V\zeta'_4) + \frac{i}{R\Gamma} (\mu\alpha_X + 2\alpha\mu_X) X$$

$$\zeta_5 + \frac{(2i \alpha\mu - U)}{R\Gamma} \zeta_{5X} - \frac{V}{\theta} \zeta_6$$

$$I_6 = -\frac{1}{\theta} (\zeta_1 + \gamma M_\infty^2 U \zeta_4 - \frac{U}{\theta} \zeta_5)$$

$$I_7 = \frac{(2ir \mu\alpha - U)}{R} \zeta_1 + \frac{1}{R} \mu' \zeta_3 + (m+1) \mu (\zeta'_3 + i\beta\zeta_7) \quad -\zeta_4$$

$$I_8 = \frac{1}{R} m\mu' \zeta_1 + (m+1) \mu \zeta'_1 + \hat{\mu} U' \zeta_5 + \frac{(2i \mu\alpha - U)}{R} \zeta_3$$

$$I_9 = \frac{i(m+1)}{R} \mu \beta \zeta_1 + \left( \frac{2i}{R} \mu \alpha - \frac{U}{\theta} \right) \zeta_7$$

$$I_{10} = (\gamma - 1) M_\infty^2 \left( \frac{2\mu U'}{R} \zeta_3 + U \zeta_4 \right) + \left( \frac{2i}{R\Gamma} \mu \alpha - \frac{U}{\theta} \right) \zeta_5$$

APPENDIX III.

The nonzero elements of the vector  $d$  in equation (32) are:

$$d_2 = \frac{iR}{\mu\theta} B_8 \zeta_1 + B_3 \zeta_2 + \frac{U'R}{\mu} \left( \frac{1}{U'} U'_{\chi} - B_1 \right) + i\alpha (B_3 + m B_4) \zeta_3$$

$$- \left( \frac{i\alpha R}{\mu^2} \mu_{\chi} + m\alpha\gamma M_{\infty}^2 B^2 \right) \zeta_4 + m\alpha B_5 - \frac{1}{\mu} (\rho U'' )_{\chi} + \frac{1}{\mu^2} \mu_{\chi} (\hat{\rho} U')_{\chi} \zeta_5$$

$$+ \left( \frac{\hat{\rho} U'}{\mu^2} \mu_{\chi} - B_6 \right) \zeta_6$$

$$d_3 = -B_4 \zeta_3 - i\gamma M_{\infty}^2 B_2 \zeta_4 + iB_5 \zeta_5$$

$$d_4 = i\alpha^2 \chi D_7 B_7 + i\alpha (2B_3 + r B_4) \zeta_1 + i\alpha^2 \chi B_7 \zeta_2 - \chi \left( \frac{r\mu'}{\mu} B_4 + \right.$$

$$\left. \frac{r\theta'}{\theta} B_3 - rB_9 + \frac{iR}{\mu\theta} B_8 + \chi D_1 B_7 \right) \zeta_3 + ir\chi\gamma M_{\infty}^2 \chi B_7 D_4 - B_2 D_2 +$$

$$(B_3 + B_4)\phi - B_{10} \zeta_4 + i\chi D_5 B_{10} D_3 \frac{r}{\theta^2} \theta_{\chi} + D_3 \left( \frac{\hat{\rho}}{\mu} \right)_{\chi} + \frac{r\mu'}{\mu\theta} B_2$$

$$- \frac{r\phi}{\theta} (B_3 + \frac{\mu'}{\mu\theta} \theta_{\chi}) - \chi B_7 D_6 \zeta_5 + ir\chi (B_5 - \frac{\chi\phi}{\theta} B_7) \zeta_6 + i\beta\chi X$$

$$(2B_3 + rB_4 + \chi D_7 B_7) \zeta_7 + i\beta\chi^2 B_7 \zeta_8$$

$$d_6 = -D_8 U'_{\chi} \zeta_2 - \left( \frac{R\Gamma}{\mu} B_4 + \frac{R\Gamma\theta'}{\mu^2} \mu_{\chi} + 2iD_8 B_{10} \right) \zeta_3 + \frac{iR}{\mu} D_8 \left( \frac{\phi}{\mu} \mu_{\chi} - B_2 \right) \zeta_4$$

$$+ \frac{iR\Gamma}{\mu\theta} B_8 - \frac{2\hat{\rho}}{\mu} D_8 (U'U'_{\chi} + W'W'_{\chi}) - D_8 (U'^2 + W'^2) \left( \frac{\hat{\rho}}{\mu} \right)_{\chi} + B_{11} \zeta_5$$

$$+ 2B_3 \zeta_6 - 2 D_6 W'_{\chi} \zeta_8$$

$$d_8 = i\beta (B_3 + m B_4) + \frac{R}{\mu\theta} (W'_{\chi} - B_1 W') \zeta_3 - \left( \frac{iR\beta}{\mu^2} \mu_{\chi} + m\beta\gamma M_{\infty}^2 B_2 \right) X$$

$$\zeta_4 + \frac{m\beta}{\theta} (B_2 - \frac{\phi}{\theta} \theta_{\chi}) - \frac{1}{\mu} (\hat{\rho} W'_{\chi})' - \frac{1}{\mu} (W' \hat{\rho}_{\chi})' - \frac{1}{\mu^2} \mu_{\chi} (\alpha W')' \zeta_5$$

$$- (W' \frac{\hat{\rho}}{\mu})_{\chi} \zeta_6 + \frac{iR}{\mu\theta} B_8 \zeta_7 + B_3 \zeta_8$$

where

$$B_1 = \frac{1}{\mu} \mu_X + \frac{1}{\theta} \theta_X$$

$$B_2 = \alpha U_X + \beta W_X$$

$$B_3 = \frac{\mu'}{\mu^2} \mu_X - \frac{1}{\mu} \mu' X$$

$$B_4 = \frac{\theta'}{\theta^2} \theta_X - \frac{1}{\theta} \theta' X$$

$$B_5 = \frac{B_2}{\theta} - \frac{\phi}{\theta^2} \theta_X$$

$$B_6 = \frac{1}{\mu} (\hat{\mu} U')_X$$

$$B_7 = i r \gamma M_\infty^2 B_2 - \frac{R}{\mu^2} \mu_X$$

$$B_8 = B_2 - \phi B_1$$

$$B_9 = \left(\frac{\theta''}{\theta}\right)_X$$

$$B_{10} = \alpha U' X + \beta W' X$$

$$B_{11} = -\left(\frac{\mu''}{\mu}\right)_X$$

and

$$D_1 = -\alpha^2 - \beta^2 + \frac{r \mu' \theta'}{\mu \theta} + \frac{r \theta''}{\theta} - \frac{i R \phi}{\mu \theta}$$

$$D_2 = \frac{\mu'}{\mu} + \frac{\theta'}{\theta}$$

$$D_3 = \alpha U' + \beta W'$$

$$D_4 = \phi D_2 + D_3$$

$$D_5 = \frac{r}{\theta} + \frac{\hat{\mu}}{\mu}$$

$$D_6 = D_3 D_5 + \frac{r \mu' \phi}{\mu \theta}$$

$$D_7 = \frac{2\mu'}{\mu} + \frac{r\theta'}{\theta}$$

$$D_8 = \Gamma (\gamma - 1) M_\infty^2$$

1. Report No. NASA CR-3474		2. Government Accession No.		3. Recipient's Catalog No.	
4. Title and Subtitle ON THE EFFECT OF BOUNDARY LAYER GROWTH ON THE STABILITY OF COMPRESSIBLE FLOWS				5. Report Date October 1981	
				6. Performing Organization Code	
7. Author(s) Nabil M. El-Hady				8. Performing Organization Report No.	
9. Performing Organization Name and Address Old Dominion University Mechanical Engineering and Mechanics Norfolk, Virginia 23508				10. Work Unit No.	
				11. Contract or Grant No. NSG-1645	
12. Sponsoring Agency Name and Address National Aeronautics and Space Administration Washington, DC 20546				13. Type of Report and Period Covered Contractor Report	
				14. Sponsoring Agency Code	
15. Supplementary Notes Langley Technical Monitor: William D. Harvey Final Report					
16. Abstract  The method of multiple scales is used to describe a formally correct method based on the nonparallel linear stability theory, that examines the two- and three-dimensional stability of compressible boundary-layer flows. The method is applied to the supersonic flat plate boundary layer at Mach number 4.5. The theoretical growth rates are in good agreement with the experimental results of Kendall. The method is also applied to the infinite-span swept wing transonic boundary layer with suction to evaluate the effect of the nonparallel flow on the development of cross-flow disturbances.					
17. Key Words (Suggested by Author(s)) Boundary layer stability Nonparallel Compressible			18. Distribution Statement Unclassified - Unlimited  Subject Category 34		
19. Security Classif. (of this report) Unclassified		20. Security Classif. (of this page) Unclassified		21. No. of Pages 45	22. Price A03